Larmor time of a bound electron wave packet tunneling through a barrier

Lijuan Jia ⓘ, Haijun Xing, and Libin Fu ⓘ*

Graduate School of China Academy of Engineering Physics, Number 10 Xibeiwang East Road, Haidian District, Beijing 100193, China

The Larmor time of an incident *wave packet* has recently been measured experimentally [R. Ramos, D. Spierings, I. Racicot, and A. M. Steinberg, Nature (London) **583**, 529 (2020)]. It differs essentially from previous well-studied free-particle cases, whereas the unique properties of wave packets are unrevealed in their theoretical analysis and state-of-the-art Larmor clock studies. In this paper, we study the Larmor time of a bound two-component electron wave packet and supplement the theoretical lack of wave-packet tunneling. We find that the spin shows a pure Larmor precession in the plane perpendicular to the field without a rotation parallel to the field. The Larmor time is defined in the limit of vanishing field where the precession angle is proportional to the field. For relatively weak fields, this precession angle will respond to the field approximately linearly. For the wave-packet tunneling case, we propose an effective scheme that utilizes the fidelity of the tunneled wave packets to calibrate an approximate linear-response region. Furthermore, we show that in the approximate linear-response region the change in the fidelity can be approximately regarded as the result of the accumulated displacement in phase space. This result reveals the inner mechanism of wave-packet tunneling. Our findings may have implications for future experiments of the Larmor clock.

I. INTRODUCTION

Quantum tunneling plays a central role in many physical contexts. The question of how much time a tunneling particle spends in a barrier forms the very crux of the tunneling problem [1]. Over decades, the efforts to define, to understand, to measure, and to interpret the value of tunneling time have been continuing by examining the scattering process of an incoming wave impinging on a potential barrier. Though no definitive answer has emerged, this has yielded a wealth of different definitions of tunneling time [2–5], such as the notable phase time [6,7], traversal time originally reported by Büttiker and Landauer [8], and complex time derived with the path-integral approach [9–11]. Among them, Larmor time [12–15] is measured via a Larmor clock.

The Larmor clock for measuring tunneling time was originally proposed by Baz' [16] and Rybachenko [17]. In their proposal, an incident spin-$\frac{1}{2}$ free particle polarized in the *x* direction moves along the *y* direction and impinges on a square barrier localized in a constant magnetic field along *z*. The particle tunneling through the barrier only performs a Larmor precession in the *x*-*y* plane and the precession angle is θ_y. This original scheme was later corrected by Büttiker [12]. Since Zeeman splitting results in the preferential tunneling, another rotation angle θ_z alignment along the antidirection of the field is triggered, as plotted in the sphere of Fig. 1. The two rotation angles in terms of the spin projections are given by [12]

$$\theta_y = -\arcsin\left(\frac{\langle S_y \rangle}{(T_\uparrow T_\downarrow)^{1/2}/(T_\uparrow + T_\downarrow)}\right), \quad (1)$$

$$\theta_z = 2\langle S_z \rangle, \quad (2)$$

where $T_{\uparrow(\downarrow)}$ is the transmitted probability of the spin-up (spin-down) component. The Larmor times are defined in the infinitesimal field limit as

$$\tau_i = \theta_i/\omega_L, \quad (3)$$

with the Larmor frequency $\omega_L = e|\mathbf{B}|/2M_e c$ and $i = y, z$, respectively. It denotes the time a particle spends in the barrier.

A generalization of the Larmor clock analysis to arbitrary potential barriers was proposed by Leavens and Aers [18]. Early measurements of Larmor times have been conducted in optical systems [19,20] and with neutrons [21], in analogy to the electronic Larmor clock. Later, the two Larmor times are found equivalent to the real and imaginary parts of the weak value of a dwell-time operator [22–24]. Notably, the Larmor times have been measured in ultracold Rb atoms with a wide range of incident energies in recent studies [13–15].

As stated above, the Larmor times of an incident particle scattering on a barrier present an ongoing development [12–15]. The Larmor times of an electron tunneling through a barrier from a quasibound state [the configuration shown in Fig. 1(b)] are still not studied. Especially, the previous studies on Larmor times were based on scattering theory; even for the case of an incident wave packet [13,15], the inner mechanism involved in the tunneling of wave packet is undiscovered. Moreover, though the time of an electron escaping from a bound state of the atom's Coulomb potential has been measured in the strong-field attosecond physics by the "attoclock" technique [25,26], the starting time of a tunneling event is hard to identify [13]. In contrast, the Larmor clock starts to tick at the time when the tunneling event starts. In this paper, we aim to measure the Larmor times of a bound electron wave packet by simulating the stationary-state evolution of the wave packet numerically and supplement the theoretical lack of wave-packet tunneling.
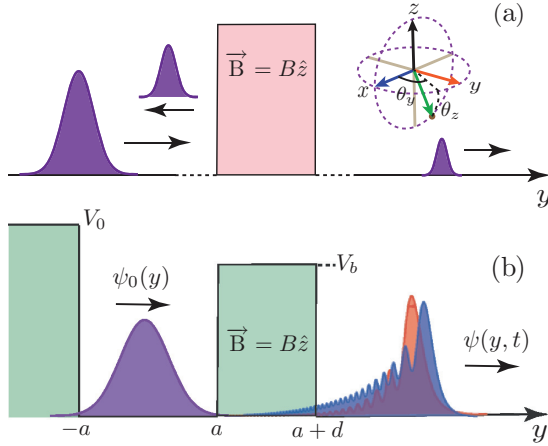
*lbfu@gscaep.ac.cn

FIG. 1. Larmor clock. (a) Scattering sketch [13]: A spin-1/2 particle, initially polarized along the x axis, hitting on a square barrier. (b) Sketch of tunneling from a quasibound state: A spin-1/2 particle is initially bounded in a square-well potential of width $2a$ and depth V_0 and polarized along the x axis, tunneling through a square barrier of width d and height V_b. A magnetic field B pointing to the z axis is confined inside the barrier. After tunneling, the spin has precessed in the x-y plane with an angle θ_y and rotated towards the antidirection of the field with an angle θ_z, as depicted in the Bloch sphere. $\psi_0(y)$ and $\psi(y, t)$ are the initial and tunneling spinors.

II. CONFIGURATION AND FORMULATION

We consider a particle trapped in a square-well potential of width $2a$ and depth V_0 ($V_0 > 0$). Initially, the particle populates at the ground state $\varphi_0(y)$ with energy E_0. At the moment $t = 0^+$, the right of the square-well potential is quenched to a square potential barrier with width d and height V_b ($V_b \ll V_0$ but $V_b > E_0$), as shown in Fig. 1(b). In this case, the particle prefers to escape from the well by tunneling through the barrier. To measure the time the particle takes inside the barrier, a uniform magnetic field $\mathbf{B}$ is localized in the barrier region. The intrinsic spin of the electron is thus a clock, which ticks only within the barrier [12,13].

A spinning charged particle constitutes a magnetic dipole. Placed in a magnetic field $\mathbf{B}$ ($\mathbf{B} = B\hat{z}$), the magnetic dipole would experience a torque. The energy associated with it is $H = -\gamma \mathbf{B} \cdot \mathbf{S}$, with the gyromagnetic ratio $\gamma = -e/M_e c$. For a particle of spin 1/2 entering into the field, the component of spin parallel to the field will have a higher energy. Equivalently, the potential barrier V_b is changed to $V_\uparrow = V_b - \omega_L/2$ ($V_\downarrow = V_b + \omega_L/2$) for the spin-up (spin-down) component. Accordingly, the total Hamiltonian of the considered system is

$$H = \begin{pmatrix} H_\uparrow & 0 \\ 0 & H_\downarrow \end{pmatrix} = \begin{pmatrix} \frac{1}{2}\frac{\partial^2}{\partial y^2} + \widetilde{V}_\uparrow & 0 \\ 0 & \frac{1}{2}\frac{\partial^2}{\partial y^2} + \widetilde{V}_\downarrow \end{pmatrix}, \quad (4)$$

with

$$\widetilde{V}_{\uparrow(\downarrow)} = \begin{cases} V_0 & y \leqslant -a, \\ 0 & -a < y \leqslant a, \\ V_{\uparrow(\downarrow)} & a < y \leqslant a + d, \\ 0 & y > a + d. \end{cases} \quad (5)$$

We denote the spinor wave function at t as

$$\psi(y, t) = \frac{1}{\sqrt{2}}\begin{pmatrix} \psi_\uparrow(y, t) \\ \psi_\downarrow(y, t) \end{pmatrix}, \quad (6)$$

with the initial wave function $\psi_\uparrow(y, 0) = \psi_\downarrow(y, 0) = \varphi_0(y)$, i.e., the particle is polarized in the x direction at $t = 0$. Since H is diagonal in this spinor basis, we can handle the time propagation of the two components separately. Their wave functions can be expanded as

$$\psi_s(y, t) = \sum_j g(\varepsilon_s^j) e^{-i\varepsilon_s^j t} \xi_s^j(y), \quad (7)$$

with $g(\varepsilon_s^j) = \int dy \xi_s^{j*}(y)\psi_s(y, 0)$ and $s = \uparrow$ and $\downarrow$, respectively, where $\xi_s^j(y)$ and ε_s^j are the eigenvectors and eigenvalues of the field-dressed Hamiltonian H_s.

When the particle tunnels out of the barrier, two rotation angles θ_y and θ_z are obtained. θ_y sources from the relative phase accumulation of the two components. Accordingly, in terms of expectation values of spin angular momentum, θ_y is defined as

$$\theta_y = -\arctan(\langle S_y \rangle / \langle S_x \rangle) \quad (8)$$

$$= -\arcsin(2\langle S_y \rangle / \sqrt{F}), \quad (9)$$

where F is the fidelity of the tunneled spin-down state $\psi_\downarrow(y)$ and spin-up state $\psi_\uparrow(y)$ given by

$$F = \left| \int dy \psi_\downarrow^*(y)\psi_\uparrow(y) \right|^2. \quad (10)$$

By measuring $\langle S_x \rangle$ and $\langle S_y \rangle$, the precession angle θ_y can be obtained in an experiment from Eq. (8), as discussed in [13]. In terms of calculating θ_y, Eq. (9) is an equivalent expression of Eq. (8). We mention that Eq. (9) is an important supplement for wave-packet tunneling since it can be utilized to infer the inner mechanism of wave-packet tunneling, as shown in Sec. IV. Furthermore, Eq. (9) is a direct generalization of Eq. (1), where the role of the different tunneling probabilities in the scattering event is replaced by the fidelity F [Eq. (10)]. In our scenario, θ_z behaves utterly different from that of the scattering event, as shown in the next section.

For the numerical results presented below, we have artificially controlled the ratio of splitting energy $\omega_L/2$ to the potential barrier V_b within 2.28%. In other words, the maximum of the field is set as 5 a.u., and $V_b = 0.8$ a.u. as a constant number throughout the calculation.

III. LARMOR PRECESSION AND LARMOR TIMES

Here, we first discuss the spin rotation angle θ_z. For the free-particle scattering event, θ_z derives from the imbalance of the constant tunneling flux with spin components $\hbar/2$ and $-\hbar/2$. The tunneling rate of each component within the barrier is also different for the case of tunneling from a quasibound state. However, the two components both tunnel out completely when the particle ends to interact with the barrier. It indicates that the population of each tunneled spinor component maintains the initial value, i.e., $\langle S_z \rangle = 0$ is conserved with integrating the tunneled spinor over the whole coordinate space. Straightforwardly, we have the Larmor time
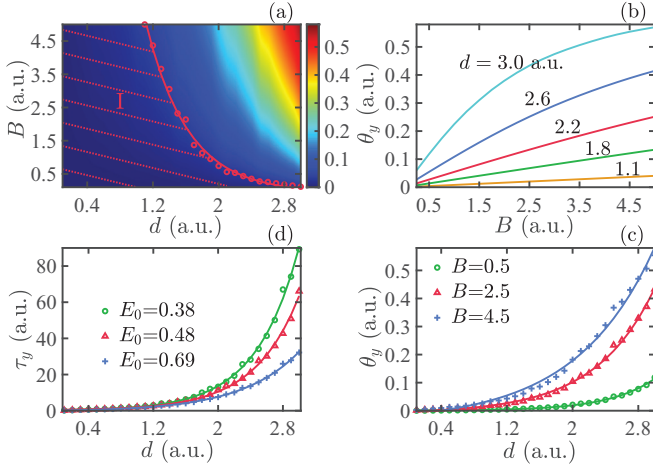
FIG. 2. (a) The Larmor precession angle θ_y. The dotted red hatched line region is the approximate linear-response region labeled as I. (b) The angle θ_y for d=1.1, 1.8, 2.2, 2.6, 3.0 a.u.. (c) The angle θ_y for B=0.5, 2.5, 4.5 a.u.. (d) The field-independent Larmor time τ_y changing with d for the cases of E_0=0.38, 0.48, 0.69 a.u..

FIG. 3. (a) Fidelity [Eq. (10)] changing with d and B. The green line (labeled as l_3) shows $F = 0.996$ a.u.. The dotted red hatched line region and the dashed purple hatched line region correspond to the linear-response region I with $\alpha = -0.1\%$ and the applicable region of Eq. (14). The blue line (labeled as l_2) is the approximate linear boundary with $\alpha = -0.02\%$. The cyan line (labeled as l_1) is $F = 0.9995$ a.u.. [(b), (c)] The distributions of spin-up (solid red line) and spin-down (dotted blue line) wave functions at d=1.5 a.u. and B=5 a.u. in (b) coordinate space and (c) momentum space. The insets show the magnified portion. δy and δp are the position and momentum differences of the highest peak of the two components. (d) For different B, the fidelity [Eq. (14)] at d=0.5 a.u. (solid green line), 1.0 a.u. (dotted red line), and 1.5 a.u. (dashed blue line) and the fidelity [Eq. (10)] at d=0.5 a.u. (green open circles), 1.0 a.u. (red triangles), and 1.5 a.u. (blue plus signs).

$\tau_z = 2\langle S_z \rangle / \omega_L = 0$. As a result, compared to the scattering event, preferential transmission of the spin component with greater energy does not trigger a spin rotation in the z direction in our scenario.

Next, we study the dependence of the Larmor precession angle θ_y on the external magnetic field B and the barrier width d. The results are plotted in Fig. 2(a). For clearness, we further select several curves that can present the changing behaviors of θ_y, plotted in Figs. 2(b) and 2(c). It shows that the response of the precession angle θ_y to the field B is not linear generally. θ_y is only approximately proportional to B for relatively weak fields. Moreover, this response behavior is also significantly affected by the barrier width d. For a fixed field, the precession angle exponentially relates to the barrier width.

Theoretically, the Larmor times are defined in the limit of the vanishing field [12]. However, the external field must be a small but finite value in a realistic experiment. For an extremely small field, the signal of measuring the Larmor precession angle will be too weak to be detected. On the other hand, increasing the field may invalidate the approximate proportional relation [Eq. (3)]. And in this case, the time obtained from Eq. (3) is incapable of measuring the time required for the particle dwelling inside the barrier. Choosing a suitable field strength is thus necessary in measuring the Larmor times.

The suitable field can be well set by identifying the region where the linear-response relation [Eq. (3)] approximately holds. As shown in Fig. 2(b), the response of the precession angle to the field behaves exponentially. Thus, there does not exist a natural linear-response region. We try to define an approximate linear-response boundary with the relative error α. $\alpha = (\theta_y - \theta_l)/\theta_l$ with $\theta_l = B\frac{\partial \theta_y}{\partial B}|_{B \to 0}$. By artificially setting $\alpha = -0.1\%$, we obtain the maximal approximate linear-response field B for different barrier widths d. Then, a boundary of approximate linear response is marked by red open circles in Fig. 2(a). It shows that a broader barrier allows a smaller maximal linear-response magnetic field. And the corresponding linear-response region (labeled as I) with
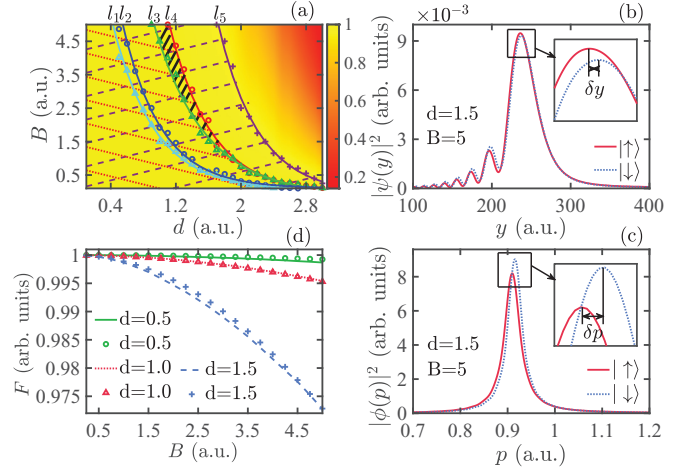
$E_0 = 0.48$ a.u. is also shown in Fig. 2(a). The Larmor time is thus well measured in this region with an accepted error. We mention that one can acquire a more precise time by setting the boundary with a smaller $|\alpha|$.

In the above discussions, we have fixed the energy E_0 ($E_0 = 0.48$ a.u.) of the initial wave packet, whereas the Larmor time is also affected by this initial energy. As depicted in Fig. 2(d), we calculate the Larmor times τ_y for different energies E_0 in the weak-field limit. It shows that the Larmor time τ_y depends on d exponentially. And τ_y becomes very sensitive to the energy E_0 at a bigger d.

IV. FIDELITY AND THE TUNNELED WAVE PACKETS

Equation (9) is regarded as the direct generalization of Eq. (1). In the free-particle scattering event, except for $\langle S_y \rangle$, the Larmor precession θ_y [Eq. (1)] is determined by the different transmission probabilities of the two components, while θ_y [Eq. (9)] is connected with the fidelity of the two tunneled wave packets for the case of tunneling from a quasibound state. Hence, fidelity is vital in analyzing the precession angle, and it can be used to study the unique properties of wave-packet tunneling. In this section, we will show these in detail.

Figure 3(a) shows the fidelity at different barrier widths and magnetic fields. It monotonously decreases with increasing d and B. This results from the fact that the two spinor

components possess different exponential decays within the barrier, which read

$$\kappa_\uparrow = \sum_j |g(\varepsilon_\uparrow^j)|^2 (2V_b - 2\varepsilon_\uparrow^j - \omega_L)^{1/2}, \quad (11)$$

$$\kappa_\downarrow = \sum_j |g(\varepsilon_\downarrow^j)|^2 (2V_b - 2\varepsilon_\downarrow^j + \omega_L)^{1/2}, \quad (12)$$

caused by the energy difference $\pm\omega_L/2$. Quantitatively, a stronger field gives rise to a bigger difference between the decay rate of each component. And a broader barrier causes more time difference between the two components tunneling out of the barrier. As a result, the average position of the wave packet for the spin-up component deviating from that of the spin-down component increases at the bigger d and B, inducing the fidelity decreases.

Since fidelity is encoded in the precession angle, the response behaviors of the precession angle to the field must be relevant with the change in fidelity. We again plot the approximate linear-response region I ($\alpha = -0.1\%$) in Fig. 3(a). On the boundary of the approximate linear response (red line labeled as l_4), the fidelity changes from 0.993 to 0.996. If the fidelity of the tunneled two components is more than 0.996, the corresponding parameter region will be the approximate linear-response region. The difference between the approximate linear-response region I and the region with $F \geqslant 0.996$ (the region to the right of the green line labeled as l_3) is quite small, as marked by the solid black hatched line in Fig. 3. Thus, the fidelity can be taken as a practical criterion to ensure the external auxiliary field is suitable and the measured time is the time required for a bound particle tunneling through the barrier. In fact, the reasonability of this criterion results from the fact that the decrease in the fidelity and the effect of nonlinear response are both caused by the different ionization rates of the two components.

Note that though the boundary of the approximate linear response is obtained artificially it is tightly associated with the inner fidelity of the system. For more explicitness, we tune the relative error $\alpha = -0.02\%$. The corresponding approximate linear-response boundary is marked by a blue line (labeled as l_2) and the maximal fidelity $F = 0.9995$ on this boundary is also marked by a cyan line (labeled as l_1) in Fig. 3(a). As expected, the difference between the line l_2 and the line l_1 is small. And, a more precise time will be measured in this recalibrated linear-response region.

As discussed above, the different tunneling rates alter the tunneled wave-packet distributions of the two spinor components, which results in the decrease in the fidelity. To discover the relative change between the two wave packets after tunneling, we plot the tunneled spinor wave functions in Figs. 3(b) and 3(c). Assuming the relative deformation is negligible, we characterize the tunneled spinor wave function as

$$\psi(y) \approx \frac{1}{\sqrt{2}} \begin{pmatrix} e^{i\theta_y/2} e^{i\frac{\delta p}{2}y} \phi\big(y + \frac{1}{2}\delta y\big) \\ e^{-i\theta_y/2} e^{-i\frac{\delta p}{2}y} \phi\big(y - \frac{1}{2}\delta y\big) \end{pmatrix}, \quad (13)$$

where $\phi(y)$ is the tunneled wave function in the absence of magnetic field. The parameters $(\delta y, \delta p)$ are the relative shift of the highest peak of spin-up and spin-down wave functions, plotted in Figs. 3(b) and 3(c). They are the functions of

magnetic field B and barrier width d. Intuitively, the relative shift δy and δp will increase for a stronger B and bigger d, which implies the descent of F. θ_y is the relative phase shift of the two components, by which the Larmor time is obtained. Expanding the approximate spinor wave function $\psi(y)$ up to the second order of δy and δp, we have the fidelity

$$F \approx 1 - \delta\mathbf{r}^{\mathrm{T}} \mathbf{g}^{\mathrm{F}} \delta\mathbf{r}, \quad (14)$$

where $\mathbf{g}^{\mathrm{F}} = \begin{pmatrix} \mathrm{Var}(p) & -\Delta \\ -\Delta & \mathrm{Var}(r) \end{pmatrix}$ is the Bures metric [27,28], with $\mathrm{Var}(a) = \langle \hat{a}^2 \rangle - \langle \hat{a} \rangle^2$, $\Delta = \mathrm{Re}\langle \hat{p}\hat{y} \rangle - \langle \hat{y} \rangle \langle \hat{p} \rangle$, and $\langle \hat{a} \rangle = \int_{-\infty}^{+\infty} dy \phi^*(y) \hat{a} \phi(y)$. $\delta\mathbf{r}^{\mathrm{T}} = (\delta y, \delta p)$ is the shift in phase space.

Compared with the fidelity calculated by Eq. (10), the fidelity resulted from Eq. (14) is also shown in Fig. 3(d) for d=0.5, 1.0, and 1.5 a.u. One can see that the results are in good agreement. Based on a unified criterion that the relative error of the approximate F [Eq. (14)] to the exact F [Eq. (10)] is 0.1%, we figure out a good agreement parameter region of this approximate spinor $\psi(y)$ for different d and B. And this region (dashed purple hatched line) is marked in Fig. 3(a), which contains the approximate linear-response region I (dotted red hatched line). This indicates that Eq. (14) is accessible in the linear-response region, where the complicated deformation is negligible, and only considering the relative displacement between the wave packets is already a well-approximated treatment. Thus, apart from the phase shift, Zeeman effect also differentiates the two spin components for wave-packet tunneling [13]. This effect of differentiation can be regarded as the displacements of the wave packets in phase space in the approximate linear-response region. This is the unique property of wave-packet tunneling and reveals the inner mechanism of the two wave packets in the tunneling process. Moreover, it is non-negligible in analyzing the Larmor process.

V. CONCLUSIONS AND DISCUSSIONS

In conclusion, distinct from the plane-wave scattering event [12], the fidelity of the tunneled two components in the wave-packet tunneling process is changed due to Zeeman splitting, henceforth encoding the fidelity in the definition of precession angle θ_y. The change in fidelity in the linear-response region can be approximately regarded as the result of accumulated displacement in phase space. This reveals the inner mechanism of wave-packet tunneling. Additionally, Zeeman splitting does not alter the z component of the spin in our scenario.

Releasing the restriction of vanishing field, the precession angle is no longer proportional to the field intensity. We have shown that the fidelity can serve as a good measure to figure out the approximate linear-response parameter space, where the Larmor time can be measured. Defining a Larmor time for the nonlinear-response case is still a worthwhile problem to be researched in the future.

We can roughly estimate the Larmor time of hydrogen atoms tunneling through a barrier in the presence of a strong field [29,30], where the barrier width can be approximately considered as 2.0 and 3.0 a.u, and the times would be around

171 and 604 as, respectively. In fact, cold atoms trapped in a quasibound state tunneling through a potential barrier have been realized experimentally [31,32]. We expect that the Larmor time needed by the atoms tunneling from a quasibound state can be measured in the system of cold atoms. Also, combining the current experiments of Larmor times [13,15], we hope that this research will inspire more studies to reveal the abundant inner mechanisms of wave-packet tunneling.

[1] L. A. MacColl, Phys. Rev. **40**, 621 (1932).

[2] R. Landauer and Th. Martin, Rev. Mod. Phys. **66**, 217 (1994).

[3] E. H. Hauge and J. A. Støvneng, Rev. Mod. Phys. **61**, 917 (1989).

[4] S. L. Alexandra and U. Keller, Phys. Rep. **547**, 1 (2015).

[5] U. S. Sainadh, R. T. Sang, and I. V. Litvinyuk, J. Phys. Photonics **2**, 042002 (2020).

[6] E. P. Wigner, Phys. Rev. **98**, 145 (1955).

[7] F. T. Smith, Phys. Rev. **118**, 349 (1960).

[8] M. Büttiker and R. Landauer, Phys. Rev. Lett. **49**, 1739 (1982).

[9] R. P. Feynman, Space-time approach to non-relativistic quantum mechanics, in *Feynman's Thesis: A New Approach To Quantum Theory*, edited by L. Brown (World Scientific, Singapore, 2005).

[10] D. Sokolovski and L. M. Baskin, Phys. Rev. A **36**, 4604 (1987).

[11] N. Yamada, Phys. Rev. Lett. **93**, 170401 (2004).

[12] M. Büttiker, Phys. Rev. B **27**, 6178 (1983).

[13] R. Ramos, D. Spierings, I. Racicot, and A. M. Steinberg, Nature (London) **583**, 529 (2020).

[14] D. C. Spierings and A. M. Steinberg, Proc. SPIE **11296**, 112960F (2020).

[15] D. C. Spierings and A. M. Steinberg, Phys. Rev. Lett. **127**, 133001 (2021).

[16] A. I. Baz', Sov. J. Nucl. Phys. **4**, 182 (1966).

[17] V. F. Rybachenko, Sov. J. Nucl. Phys. **5**, 635 (1967).

[18] C. R. Leavens and G. C. Aers, Solid State Commun. **63**, 1101 (1987).

[19] M. Deutsch and J. E. Golub, Phys. Rev. A **53**, 434 (1996).

[20] Ph. Balcou and L. Dutriaux, Phys. Rev. Lett. **78**, 851 (1997).

[21] M. Hino, N. Achiwa, S. Tasaki, T. Ebisawa, T. Kawai, T. Akiyoshi, and D. Yamazaki, Phys. Rev. A **59**, 2261 (1999).

[22] Y. Aharonov, D. Z. Albert, and L. Vaidman, Phys. Rev. Lett. **60**, 1351 (1988).

[23] A. M. Steinberg, Phys. Rev. Lett. **74**, 2405 (1995).

[24] C. A. A. de Carvalho and H. M. Nussenzveig, Phys. Rep. **364**, 83 (2002).

[25] Eckle, P., M. Smolarski, P. Schlup, J. Biegert, A. Staudte, M. Schöffler, H. G. Muller, R. Dörner, and U. Keller, Nat. Phys. **4**, 565 (2008).

[26] Eckle, P., A. N. Pfeiffer, C. Cirelli, A. Staudte, R. Dörner, H. G. Muller, M. Büttiker, and U. Keller, Science **322**, 1525 (2008).

[27] D. J. C. Bures, Trans. Am. Math. Soc. **135**, 199 (1969).

[28] We mention that the Bures metric is a quarter of the quantum Fisher information that plays significant roles in the quantum parameter estimation.

[29] U. S. Sainadh, H. Xu, X. Wang, A. Atia-Tul-Noor, W. C. Wallace, N. Douguet, A. Bray, I. Ivanov, K. Bartschat, A. Kheifets, R. T. Sang, and I. V. Litvinyuk, Nature (London) **568**, 75 (2019).

[30] L. Torlina, F. Morales, J. Kaushal, I. Ivanov, A. Kheifets, A. Zielinski, A. Scrinzi, H. G. Muller, S. Sukiasyan, M. Ivanov, and O. Smirnova, Nat. Phys. **11**, 503 (2015).

[31] S. Potnis, R. Ramos, K. Maeda, L. D. Carr, and A. M. Steinberg, Phys. Rev. Lett. **118**, 060402 (2017).

[32] X. Zhao, D. A. Alcala, M. A. McLain, K. Maeda, S. Potnis, R. Ramos, A. M. Steinberg, and L. D. Carr, Phys. Rev. A **96**, 063601 (2017).